PHYSICAL REVIEW D VOLUME 30, NUMBER 6 15 SEPTEMBER 1984

Illustrated study of flux patterns in SU(2) lattice gauge theory

Joe Kiskis and Kevin Sparks
Department of Physics, University of California at Davis, Davis, California 95616
(Received 19 April 1984)

Flux patterns in four-dimensional, SU(2) lattice gauge theory are studied with Monte Carlo simulation. The flux correlations associated with elementary, three-dimensional cubes are presented as stereo pictures of the flux vectors. Comparisons with lowest-order, weak-coupling, and $U(1)\times U(1)\times U(1)$ Monte Carlo results are made. The fluctuations of the SU(2) theory are larger and more disordered than those of the comparison systems.

I. INTRODUCTION

This paper reports on continuing numerical studies of SU(2) lattice-gauge-field configurations first presented in Ref. 1 (to be referred to as I). The goal is to develop physical insight into the behavior of non-Abelian gauge fields. Work of this type can test ideas concerning important field configurations and may suggest unexpected directions for further research.

The theory[2] is controlled by local dynamics so, in principle, the long-distance properties are in some way present at short distance. The renormalization group propagates them out to large distance. In practice, little is known about this behavior. We begin with a look at the flux patterns around elementary $1\times 1\times 1$ cubes. These are interesting and still simple enough to study in detail.

In I, some initial results were presented. It was found that significant, non-Abelian effects in elementary cubes persisted at large values of β. A more detailed study is described here. Enough information is collected so that the data can be represented as stereo pictures of the flux vectors associated with cubes. As in I, the lattice is of size 10^4 and the β values range from 2.0 to 5.2.

To interpret the data, it is useful to have simpler systems for comparison. In I, lowest-order weak-coupling calculations provided a baseline. This essentially Abelian limit of the theory will also be used here. In addition, it is interesting to compare with a full Abelian theory. The $U(1)\times U(1)\times U(1)$ theory has the same number of degrees of freedom as the SU(2) theory. The numerical simulation of it produces data that provide an additional point of reference for the SU(2) results. Qualitative effects attributable to the non-Abelian interactions are then easy to spot.

The conclusion of this study is that the flux pattern is significantly non-Abelian over the whole β range. This range includes large β values and thus very small physical sizes for the elementary cubes. More specifically the non-Abelian interactions in SU(2) give larger and more disordered fluctuations than are found in the Abelian comparison systems. We do not know if this disordering is of the type[3] that has been shown to be associated with an area law for the Wilson loop.

Section II discusses the theoretical motivation and the weak-coupling calculations. Section III presents numerical results for SU(2) and $U(1)\times U(1)\times U(1)$. They are displayed in graphs and pictures. Section IV interprets these data and relates them to results in I. Section V briefly restates the general conclusion.

II. THEORETICAL DISCUSSION

This section reviews the flux concepts, introduces the flux averages of interest, and describes calculations in the weak-coupling limit.

A. Flux

Our basic ideas for the study of flux have been described in I and Ref. 4. Gauge invariance requires that different plaquette flux vectors be parallel transported to the same site for comparison. Thus, to study the patterns in a three-dimensional cube, consider Fig. 1 and the routes $r_1, \ldots, r_6$ each associated with a face and all based at the same site. Given a gauge-field configuration, an element $U(r_i)$ of the gauge group is associated with each route as usual. These group elements can be parametrized by a vector of angles

$$U(r_i)=e^{i\vec{\theta}_i\cdot\vec{\sigma}} \tag{2.1}$$

with

$$0\leq |\vec{\theta}_i| \leq \pi\ . \tag{2.2}$$

$\vec{\theta}_i$ will be referred to as the flux through face i. The magnitude of the flux is gauge invariant. The orientation

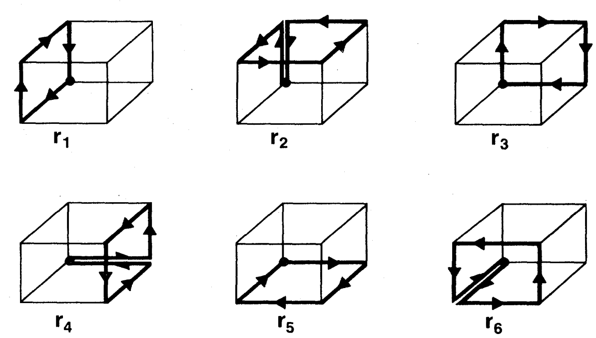

FIG. 1. An elementary cube and the routes r_i associated with the ith face.

is meaningful only in comparison with the other flux vectors based at the same site.

The relationships among these vectors can be studied in considerable detail. For example, it is straightforward to extract and plot the six flux vectors associated with a given cube in a given field configuration. Unfortunately, this is not very instructive. Even for adjacent faces at large β, the tendency of the vectors to align or antialign is small. The eye misses the small correlations. It is necessary to consider appropriately chosen averages.

In I, the averages $\langle \vec{\theta}_1\cdot\vec{\theta}_i \rangle$ were studied. Here we obtain the more detailed information needed to construct pictures of the six flux vectors associated with a given cube. Simple averages of the vectors $\vec{\theta}_i$ are not gauge invariant. It is only relative orientations, not absolute orientations, that are meaningful. To proceed, choose an orthonormal basis $\hat{\phi}_1$, $\hat{\phi}_2$, $\hat{\phi}_3$ fixed relative to $\vec{\theta}_1$ and $\vec{\theta}_3$:

$$\begin{aligned}&\hat{\phi}_1\equiv\hat{\theta}_1 ,\\ &\hat{\phi}_2\equiv(\vec{\theta}_3-\hat{\theta}_1\hat{\theta}_1\cdot\vec{\theta}_3)/\,|\,\vec{\theta}_3-\hat{\theta}_1\hat{\theta}_1\cdot\vec{\theta}_3\,| ,\\ &\hat{\phi}_3\equiv\hat{\phi}_1\times\hat{\phi}_2=\vec{\theta}_1\times\vec{\theta}_3/\,|\,\vec{\theta}_1\times\vec{\theta}_3\,| .\end{aligned} \tag{2.3}$$

This is a right-handed coordinate system oriented so that $\vec{\theta}_1$ has only a positive 1-component and $\vec{\theta}_3$ has only a 1-component and a positive 2-component. The new components $\hat{\phi}_i\cdot\vec{\theta}_j$ of $\vec{\theta}_j$ can be computed. Viewing individual configurations of vectors in this basis is no more enlightening than in the original basis. But now it is meaningful to compute the averages

$$\langle \hat{\phi}_i\cdot\vec{\theta}_j \rangle,\quad i=1,2,3,\quad j=1,\ldots,6 \tag{2.4}$$

that reveal patterns in the flux. The pictures are a representation of the average vectors in the new "body-fixed" basis.

To obtain a more quantitative understanding of this information, two comparisons are helpful. The weak-coupling limit of the averages in (2.4) can be computed and compared with the measurements. It is also interesting to compare the non-Abelian SU(2) theory to an Abelian theory with the same number of degrees of freedom: $U(1)\times U(1)\times U(1)$. Since we follow the usual definitions and conventions, it is appropriate to make the comparison at the same β values. The effect of non-Abelian interactions on the flux pattern can be seen quite directly.

B. Weak coupling

The lowest-order, weak-coupling calculation in SU(2) is essentially Abelian. Each color component fluctuates independently and can be thought of as a separate U(1) theory. Thus, at the same β, the lowest-order results for SU(2) and $U(1)\times U(1)\times U(1)$ coincide.

In I, standard methods were used to calculate $\langle \vec{\theta}_1\cdot\vec{\theta}_j \rangle$. Now consider

$$\langle \hat{\phi}_1\cdot\vec{\theta}_j \rangle=\langle \vec{\theta}_1\cdot\vec{\theta}_j(\vec{\theta}_1\cdot\vec{\theta}_1)^{-1/2} \rangle . \tag{2.5}$$

Since this is not a polynomial or even expressible as a power series in the link variables, it cannot be handled directly. However, the identity

$$A^{-1/2}=(2\pi)^{-1/2}\int d\gamma\, e^{-\gamma^2 A/2} \tag{2.6}$$

can be used to write

$$\langle \hat{\phi}_1\cdot\vec{\theta}_j \rangle=(2\pi)^{-1/2}\int d\gamma \langle e^{-\gamma^2\vec{\theta}_1\cdot\vec{\theta}_1/2}\vec{\theta}_1\cdot\vec{\theta}_j \rangle . \tag{2.7}$$

It is convenient to introduce another dummy integration so that

$$\langle \hat{\phi}_1\cdot\vec{\theta}_j \rangle=(2\pi)^{-2}\int d\gamma \int d^3\beta\, e^{-\beta^2/2}\langle e^{i\gamma\vec{\beta}\cdot\vec{\theta}_1}\vec{\theta}_1\cdot\vec{\theta}_j \rangle . \tag{2.8}$$

Now the usual methods[5] can be applied to the average in (2.8). Luckily, the final γ and β integrations are elementary. The average $\langle \hat{\theta}_1\cdot\hat{\theta}_3 \rangle$, which will be of interest later, can be handled similarly.

The method does not work on $\langle \hat{\phi}_2\cdot\vec{\theta}_j \rangle$ because of a more complicated denominator:

$$\begin{aligned}\langle \hat{\phi}_2\cdot\vec{\theta}_j \rangle&=\langle (\vec{\theta}_3\cdot\vec{\theta}_j-\vec{\theta}_3\cdot\hat{\theta}_1\hat{\theta}_1\cdot\vec{\theta}_j)\\ &\quad\times[\vec{\theta}_3\cdot\vec{\theta}_3-(\hat{\theta}_1\cdot\vec{\theta}_3)^2]^{-1/2} \rangle &(2.9)\\ &=\langle (\vec{\theta}_1\cdot\vec{\theta}_1\vec{\theta}_3\cdot\vec{\theta}_j-\vec{\theta}_3\cdot\vec{\theta}_1\vec{\theta}_1\cdot\vec{\theta}_j)(\vec{\theta}_1\cdot\vec{\theta}_1)^{-1/2}\\ &\quad\times(\vec{\theta}_1\cdot\vec{\theta}_1\vec{\theta}_3\cdot\vec{\theta}_3-\vec{\theta}_1\cdot\vec{\theta}_3\vec{\theta}_1\cdot\vec{\theta}_3)^{-1/2} \rangle . &(2.10)\end{aligned}$$

One can use (2.6) to deal with the $(\vec{\theta}_1\cdot\vec{\theta}_1)^{-1/2}$ factor. If (2.6) is applied to the other square-root factor, an intractable quartic exponent is obtained. This difficulty is overcome with the observation that

$$\vec{\theta}_1\cdot\vec{\theta}_1\vec{\theta}_3\cdot\vec{\theta}_3-\vec{\theta}_1\cdot\vec{\theta}_3\vec{\theta}_1\cdot\vec{\theta}_3=\det A \tag{2.11}$$

when

$$A=\begin{bmatrix}\vec{\theta}_1\cdot\vec{\theta}_1 & \vec{\theta}_1\cdot\vec{\theta}_3\\ \vec{\theta}_1\cdot\vec{\theta}_3 & \vec{\theta}_3\cdot\vec{\theta}_3\end{bmatrix} . \tag{2.12}$$

Now if α is a two-component column vector, then

$$(\det A)^{-1/2}=(2\pi)^{-1}\int d^2\alpha\, e^{-\alpha^T A\alpha/2} . \tag{2.13}$$

Furthermore,

$$\alpha^T A\alpha=(\alpha_1\vec{\theta}_1+\alpha_2\vec{\theta}_3)^2 \tag{2.14}$$

and thus

$$e^{-\alpha^T A\alpha/2}=(2\pi)^{-3/2}\int d^3\sigma \exp[-\tfrac{1}{2}\sigma^2+i(\alpha_1\vec{\theta}_1+\alpha_2\vec{\theta}_3)\cdot\vec{\sigma}] . \tag{2.15}$$

The result of all this is another expression that can be attacked in the usual way:

$$\begin{aligned}\langle \hat{\phi}_2\cdot\vec{\theta}_j \rangle=(2\pi)^{-9/2}\int d\gamma\int d^2\alpha\int d^3\beta\int d^3\sigma\, e^{-(\beta^2+\sigma^2)/2}\\ \times\langle \exp[i\gamma\vec{\theta}_1\cdot\vec{\beta}+i(\alpha_1\vec{\theta}_1+\alpha_2\vec{\theta}_3)\cdot\vec{\sigma}](\vec{\theta}_1\cdot\vec{\theta}_1\vec{\theta}_3\cdot\vec{\theta}_j-\vec{\theta}_3\cdot\vec{\theta}_1\vec{\theta}_1\cdot\vec{\theta}_j) \rangle .\end{aligned} \tag{2.16}$$

The gauge-field averages in (2.8) and (2.16) are Gaussian in lowest order. They were done for an infinite lattice. The necessary propagators were obtained by doing one momentum integration analytically and the remaining three numerically. The results at order $1/\sqrt{\beta}$ are

$$\langle \hat{\phi}_1 \cdot \vec{\theta}_1 \rangle = 1.13/\sqrt{\beta} , \tag{2.17a}$$

$$\langle \hat{\phi}_1 \cdot \vec{\theta}_j \rangle = -0.244/\sqrt{\beta} , \quad j = 2,3,5,6 \tag{2.17b}$$

$$\langle \hat{\phi}_1 \cdot \vec{\theta}_4 \rangle = -0.155/\sqrt{\beta} , \tag{2.17c}$$

$$\langle \hat{\phi}_2 \cdot \vec{\theta}_1 \rangle = 0 , \tag{2.17d}$$

$$\langle \hat{\phi}_2 \cdot \vec{\theta}_j \rangle = -0.238/\sqrt{\beta}, \quad j = 2,5 \tag{2.17e}$$

$$\langle \hat{\phi}_2 \cdot \vec{\theta}_3 \rangle = 0.865/\sqrt{\beta} , \tag{2.17f}$$

$$\langle \hat{\phi}_2 \cdot \vec{\theta}_4 \rangle = -0.223/\sqrt{\beta} , \tag{2.17g}$$

$$\langle \hat{\phi}_2 \cdot \vec{\theta}_6 \rangle = -0.166/\sqrt{\beta} , \tag{2.17h}$$

$$\langle \hat{\theta}_1 \cdot \hat{\theta}_3 \rangle = -0.184 . \tag{2.17i}$$

The relative sizes of the averages in (2.17) give information about typical weak-coupling flux configurations that can be understood in terms of the geometry of the cube. Faces 2, 3, 5, and 6 are all adjacent to face 1 while 4 is across the cube. Thus, (2.17b) and (2.17c) indicate that the flux exiting any face next to face 1 is equally likely to be oriented parallel to the flux entering face 1 and that the flux exiting the more distant face 4 is somewhat less likely to be so oriented. By construction, $\hat{\phi}_2$ is orthogonal to $\vec{\theta}_1$ and determined otherwise by $\vec{\theta}_3$. This easily explains (2.17d) and (2.17f). Since faces 2 and 5 are adjacent to and symmetrically placed relative to faces 3 and 1, the equality in (2.17e) is understood. Face 4 is adjacent to face 3 but opposite face 1, while face 6 is opposite face 3 and next to the less important face 1. This rationalizes the relative sizes of (2.17e), (2.17g), and (2.17h).

A simple consequence of the lowest-order version of the Bianchi identity[1,4,6] is

$$\left\langle \hat{\phi}_i \cdot \sum_{j=1}^{6} \vec{\theta}_j \right\rangle = 0, \quad i = 1,2 . \tag{2.18}$$

The results in (2.17) satisfy this constraint. It expresses the conservation of flux in an Abelian approximation. The U(1)×U(1)×U(1) theory will satisfy (2.18) in every order.

Now consider

$$\langle \hat{\phi}_3 \cdot \vec{\theta}_j \rangle = \langle \vec{\theta}_1 \times \vec{\theta}_3 \cdot \vec{\theta}_j / | \vec{\theta}_1 \times \vec{\theta}_3 | \rangle . \tag{2.19}$$

The lowest-order contribution to this average is zero since the different color directions fluctuate independently. This is also true to all orders in the U(1)×U(1)×U(1) theory. In SU(2), there will be nonzero contributions in the next order where interactions among the color directions take place. This average is a measure of the importance of these interactions.

III. NUMERICAL RESULTS

In the previous section, some flux averages were introduced. The Monte Carlo data are presented in this section. The interpretation will be given in Sec. IV.

The SU(2) averages are from the configurations described in I, and the numerical methods were discussed there. The lattice is of size 10^4 and the β values are 2.0, 2.4, 2.6, 3.0, 3.5, and 5.2.

The lattice size for the U(1)×U(1)×U(1) work is also 10^4; the β values are 2.0, 2.6, and 5.2. A heat-bath algorithm outlined by Caldi[7] was used to generate configurations from an ordered start. A U(1)×U(1)×U(1) configuration consists of three independent U(1) configurations. Otherwise the sampling is similar to that in I. Averages were separated by five sweeps after an initial 30—35 sweeps. Also at $\beta=2.0$ and 5.2, the quantities of interest were measured every five sweeps from the ordered start. This was done to check for trends in the averages versus iteration number. After the first two measurements no trends were seen, and we conclude that the lattices were adequately thermalized by 30—35 iterations.

The SU(2) flux for some randomly selected cubes was computed. Two examples at $\beta=2.6$ are shown in Fig. 2. These are stereo views. To perceive the depth information, hold the figure squarely oriented and about ten inches from your eyes. In looking at this page, your eyes are pointing so that the two lines-of-sight intersect on the page. To view the figures, cross your eyes slowly so that the lines-of-sight intersect in front of the page. As you do so, each view will split, and you will see four rather than two sets of vectors. Continue this until the center pair fuse into a new image. It seems to help to frown a little and concentrate on the centers of the figures. This takes a couple of minutes of practice and adjustment, but when the images lock together, the effect is dramatic and quite three-dimensional.

In Figs. 3(a)—3(i), the SU(2) and U(1)×U(1)×U(1) data for $\langle \hat{\phi}_i \cdot \vec{\theta}_j \rangle$, $(i,j)=(1,1)$, (2,3), (1,3), (1,4), (2,5), (2,4), (2,6), (3,5), and (3,4) are shown. (1,2) is not shown because it does not (as it should not) differ significantly from (1,3). Similar statements hold for the other missing (i,j) values. The curves are the lowest-order, weak-coupling results.

As an example of $\langle \hat{\theta}_1 \cdot \hat{\theta}_j \rangle$ data, $\langle \hat{\theta}_1 \cdot \hat{\theta}_3 \rangle$ is given in Fig.

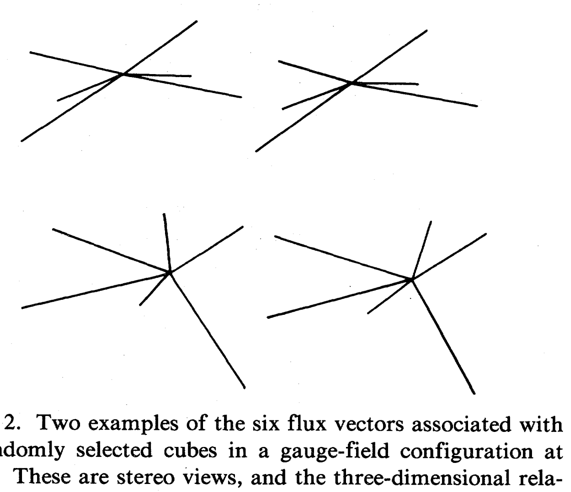

FIG. 2. Two examples of the six flux vectors associated with two randomly selected cubes in a gauge-field configuration at $\beta=2.6$. These are stereo views, and the three-dimensional relationships can be perceived by following instructions in the text. The overall orientation of the figures and the labeling of the vectors are not relevant here.

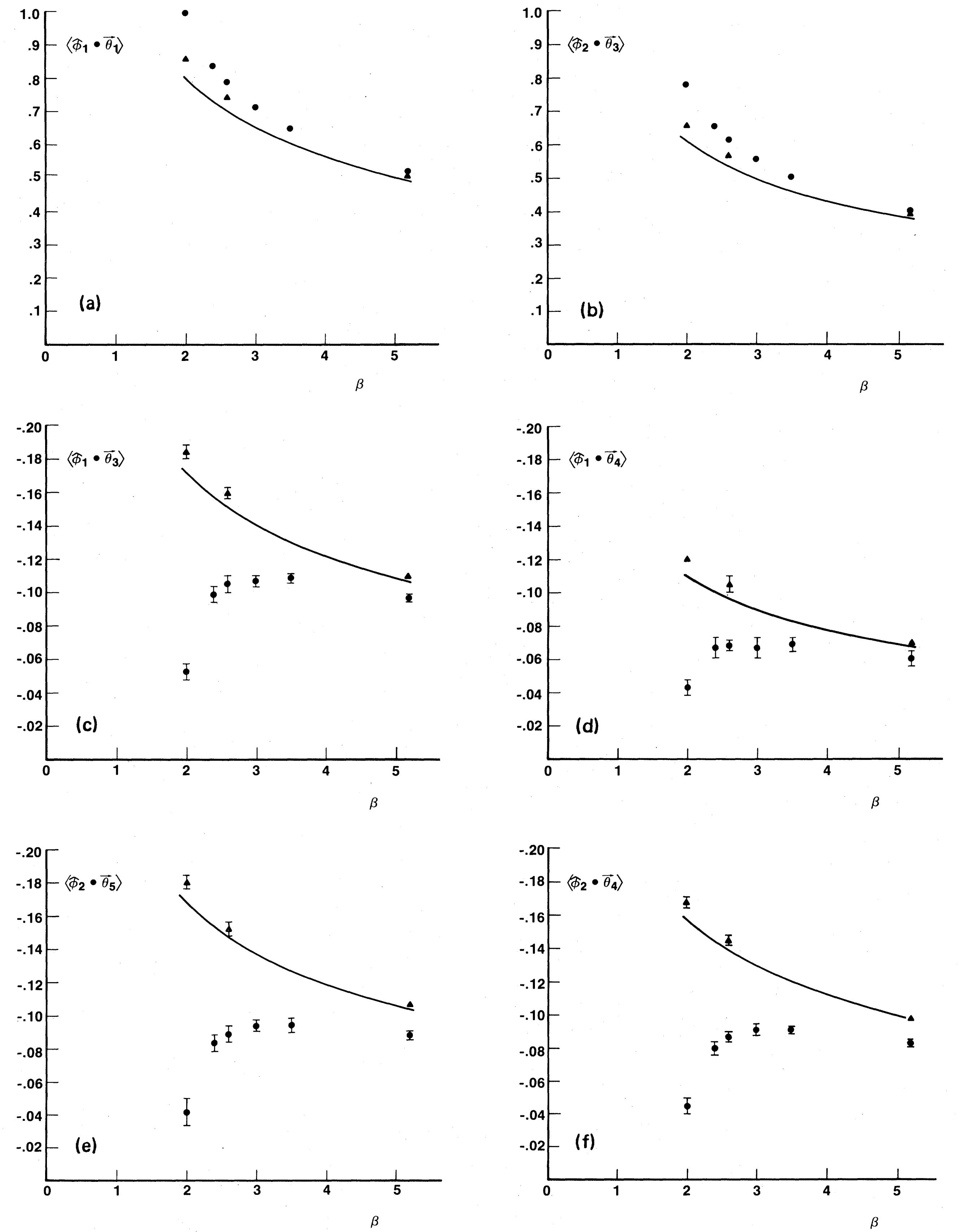

FIG. 3. Graphs of $\langle \hat{\phi}_i \cdot \vec{\theta}_j \rangle$ vs β. The dots are SU(2) data, the triangles are U(1)×U(1)×U(1) data, and the curves are the weak-coupling results of (2.17). The (i,j) values are (a) (1,1), (b) (2,3), (c) (1,3), (d) (1,4), (e) (2,5), (f) (2,4), (g) (2,6), (h) (3,5), (i) (3,4).

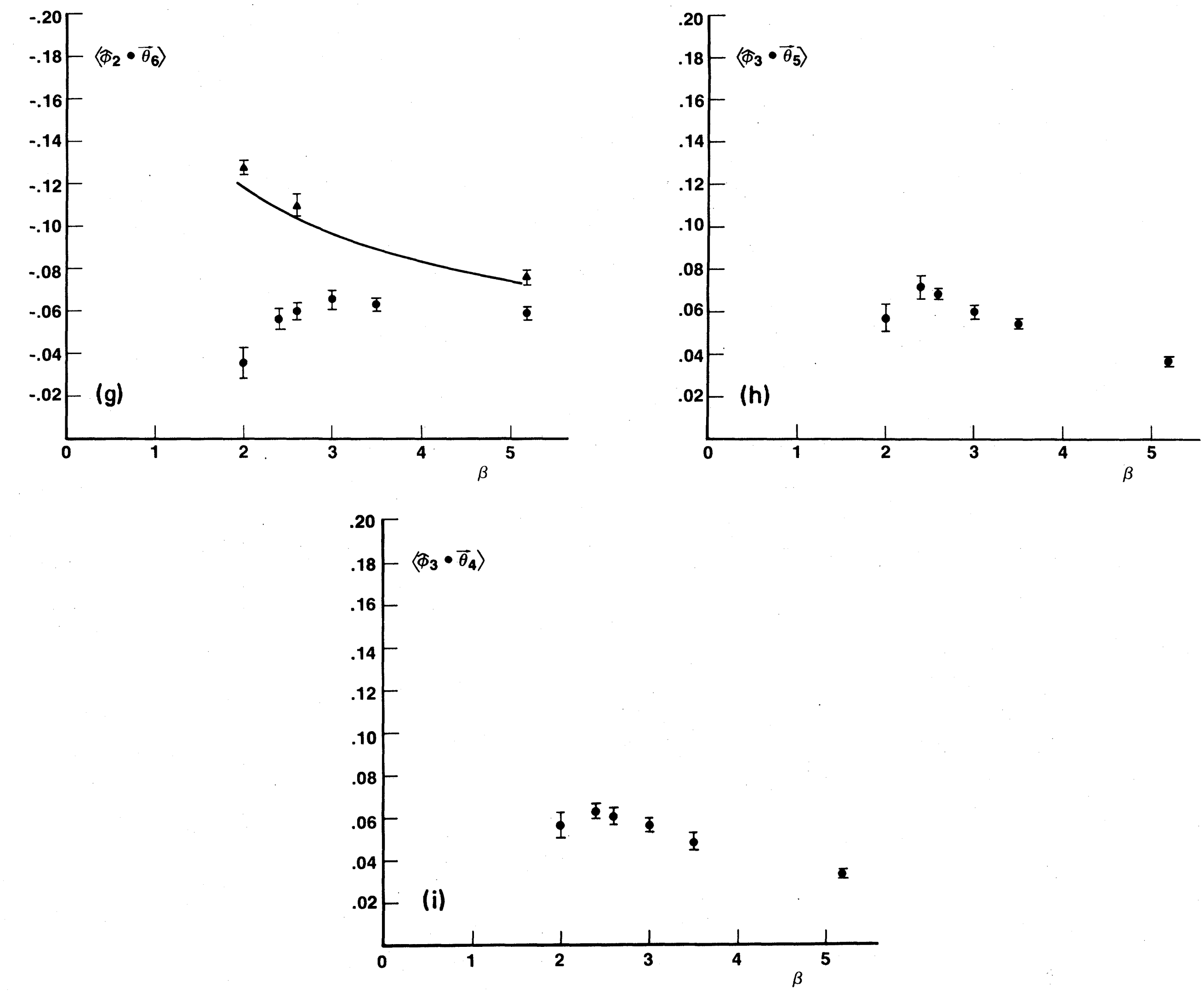

FIG. 3. (*Continued*).

4. The lower points are SU(2), the upper ones U(1) $\times$U(1)$\times$U(1), and the line is the weak-coupling result.

The $\langle \hat{\phi}_i \cdot \vec{\theta}_j \rangle$ data can be represented in terms of pictures that show the average orientations of the six flux vectors relative to the $\hat{\phi}_i$ basis. Results for SU(2) at β=2.0, 2.6, and 5.2 are given in Fig. 6. Figure 5 is a reference to indicate labeling that would overly clutter the stereo views in Figs. 6 and 7. The U(1)$\times$U(1)$\times$U(1) average vectors are drawn in Fig. 7, and all $\langle \hat{\phi}_3 \cdot \vec{\theta}_j \rangle$ vanish in this case. In both cases, the larger vectors $\vec{\theta}_1$ and $\vec{\theta}_3$ are scaled down by a factor of 10. Although the overall scales of the printed figures vary slightly, the coordinate axes always represent a length of 0.10.

IV. INTERPRETATION

Examples of flux configurations such as those in Fig. 2 look random. This is because they are not too far from random. Although the correlations are qualitatively important, they are small quantitatively. One way to see this is to consider the measured values of $\langle \hat{\theta}_1 \cdot \hat{\theta}_3 \rangle$ in Fig. 4. They are not only much less than one, but for SU(2), also

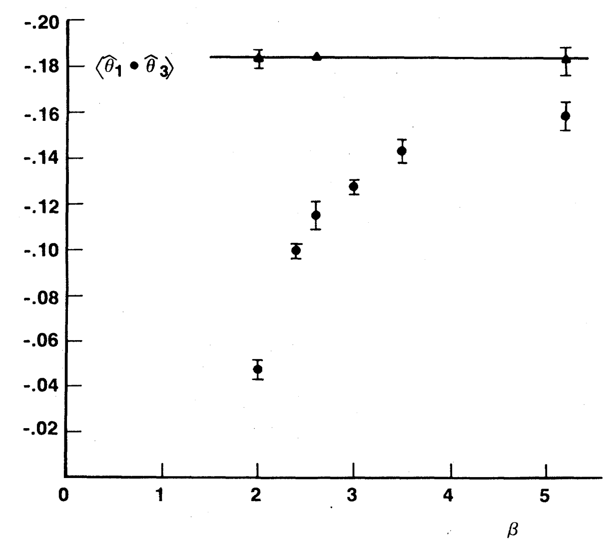

FIG. 4. Graph of $\langle \hat{\theta}_1 \cdot \hat{\theta}_3 \rangle$ vs β. The dots are SU(2) data, the triangles are U(1)$\times$U(1)$\times$U(1) data, and the line is the weak-coupling result.

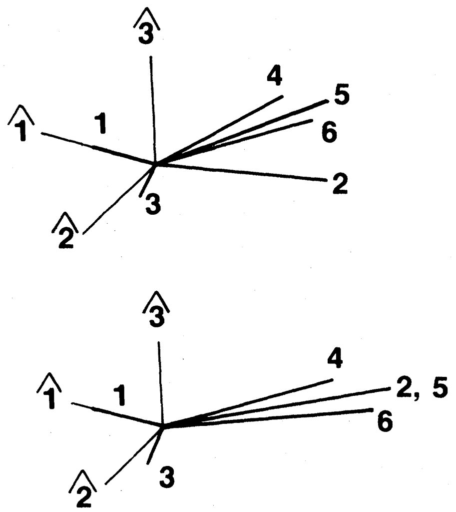

FIG. 5. Labeling for Figs. 6 and 7.

well below the weak-coupling number. There is only a small tendency for $\vec{\theta}_1$ and $\vec{\theta}_3$ to antialign. Similar conclusions apply to the other faces of the cube.

The small alignments can be seen in the average projections of the flux vectors onto the $\hat{\phi}_i$ basis. Consider $\langle \hat{\phi}_1 \cdot \vec{\theta}_1 \rangle$ first. Since

$$\langle \hat{\phi}_1 \cdot \vec{\theta}_1 \rangle = \langle \, | \vec{\theta}_1 | \, \rangle = \langle \, | \vec{\theta}_i | \, \rangle \ , \tag{4.1}$$

this quantity is an indication of the size of the fluctuations of the flux through a single plaquette. The SU(2) data of Fig. 3(a) are above the weak-coupling curve and above the $U(1)\times U(1)\times U(1)$ data. Thus, the effect of

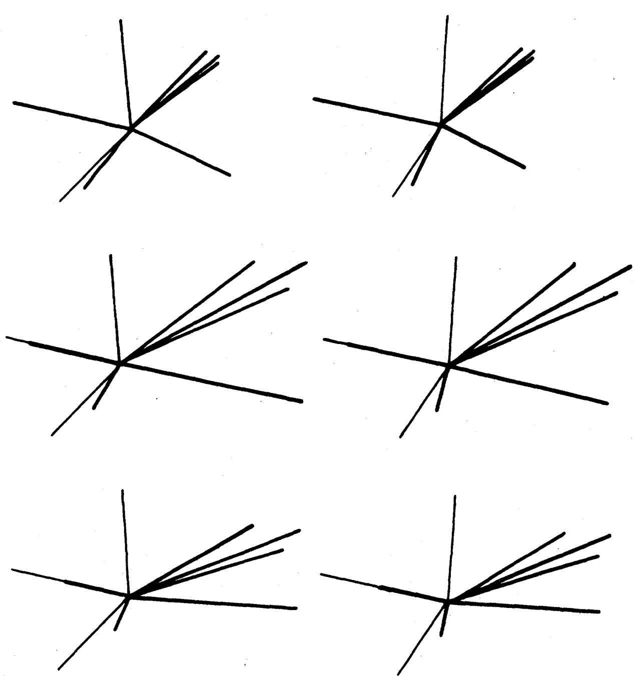

FIG. 6. Stereo views of $\langle \hat{\phi}_i \cdot \vec{\theta}_j \rangle$ for SU(2). The top, middle, and bottom pictures are $\beta=2.0$, 2.6, and 5.2, respectively. The $\vec{\theta}_1$ and $\vec{\theta}_3$ vectors are shown at $\frac{1}{10}$ of their true length. The coordinate axes represent a length of 0.10.

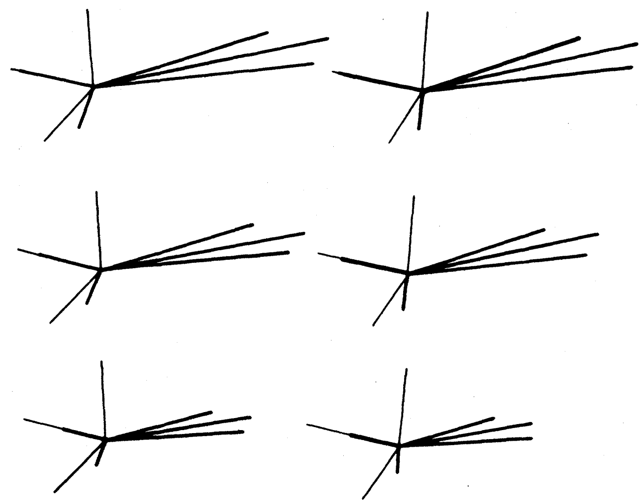

FIG. 7. Stereo views of $\langle \hat{\phi}_i \cdot \vec{\theta}_j \rangle$ for $U(1)\times U(1)\times U(1)$ as per Fig. 6. In this case, all vectors are in the 1,2 plane.

non-Abelian interactions is to increase the average magnitude of the flux. Similar statements apply to $\langle \hat{\phi}_2 \cdot \vec{\theta}_3 \rangle$, which is the magnitude of the component of $\vec{\theta}_3$ perpendicular to $\vec{\theta}_1$. See Fig. 3(b).

$\langle \hat{\phi}_1 \cdot \vec{\theta}_3 \rangle$ and the other averages shown in Figs. 3(c)—3(g) measure the flux alignments around the cube. The SU(2) data are below the weak-coupling curves and below the $U(1)\times U(1)\times U(1)$ data. This indicates that the effect of the non-Abelian interactions is to disorder the flux pattern.

The weak-coupling approximation to the averages in Figs. 3(c)—3(g) is not very close to the measured values. This is probably due to the fact that $\langle \hat{\theta}_1 \cdot \hat{\theta}_3 \rangle$ and the other similar quantities are so far below the weak-coupling value. Here is another indication of the substantial disordering of the flux even at moderately large β values.

Now consider the averages $\langle \hat{\phi}_3 \cdot \vec{\theta}_i \rangle$. In SU(2), they are zero in the lowest-order weak-coupling calculations. In the next order, when the three-gluon vertex is included, they will get nonzero contributions. In the $U(1)\times U(1)\times U(1)$ theory, these averages are exactly zero. Thus they can be thought of as a measure of the non-Abelianness of the flux configuration.

$\langle \hat{\phi}_3 \cdot \vec{\theta}_1 \rangle$ and $\langle \hat{\phi}_3 \cdot \vec{\theta}_3 \rangle$ vanish by construction. $\langle \hat{\phi}_3 \cdot \vec{\theta}_5 \rangle$ is shown in Fig. 3(h) and is positive. The data for $\langle \hat{\phi}_3 \cdot \vec{\theta}_2 \rangle$ do not differ significantly from those in Fig. 3(h) except that the sign is negative. $\langle \hat{\phi}_3 \cdot \vec{\theta}_4 \rangle$ and $\langle \hat{\phi}_3 \cdot \vec{\theta}_6 \rangle$ are positive and indistinguishable. $\langle \hat{\phi}_3 \cdot \vec{\theta}_4 \rangle$ is in Fig. 3(i) and may be slightly below $\langle \hat{\phi}_3 \cdot \vec{\theta}_5 \rangle$.

The pattern of signs in these four averages can be understood. For example,

$$\langle \hat{\phi}_3 \cdot \vec{\theta}_5 \rangle = \langle \hat{\phi}_1 \times \hat{\phi}_2 \cdot \vec{\theta}_5 \rangle = \langle \vec{\theta}_1 \times \vec{\theta}_3 \cdot \vec{\theta}_5 / \, | \vec{\theta}_1 \times \vec{\theta}_3 | \, \rangle \tag{4.2}$$

is associated with the route $r = r_5 r_3 r_1$ shown in Fig. 8. A short calculation shows that a positive sign in (4.2) has the effect of decreasing the flux through r. The signs for the

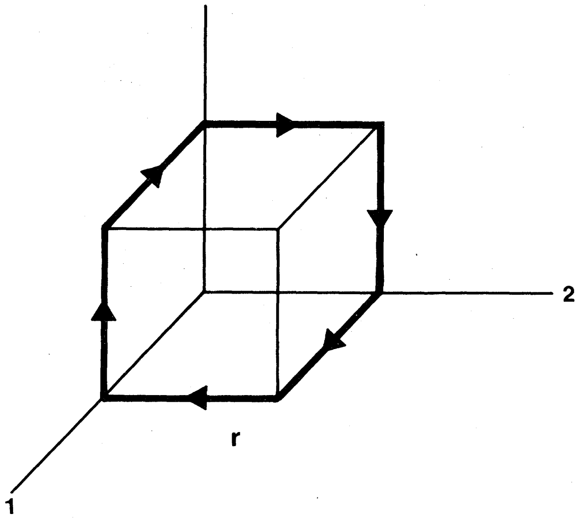

FIG. 8. An elementary cube and the route $r = r_5 r_3 r_1$.

other three averages follow from similar reasoning.

That

$$|\langle \hat{\phi}_3 \cdot \vec{\theta}_5 \rangle| \cong |\langle \hat{\phi}_3 \cdot \vec{\theta}_2 \rangle| \quad (4.3)$$

is not surprising given that faces 2 and 5 are the same distance from faces 1 and 3. That

$$\langle \hat{\phi}_3 \cdot \vec{\theta}_4 \rangle \cong \langle \hat{\phi}_3 \cdot \vec{\theta}_6 \rangle \quad (4.4)$$

and may be slightly smaller than (4.3) can be rationalized with the observation that faces 4 and 6 are similarly related to faces 1 and 3 and are each farther from faces 1 and 3 than are faces 2 and 5.

More importantly, one should note that the data in Figs. 3(h) and 3(i) certainly are not negligible compared to those in Figs. 3(c)—3(g). So even at rather large β values, there are significant non-Abelian features in the single-cube flux pattern.

This information can be presented in the flux pictures of Figs. 6 and 7. $\langle \hat{\phi}_1 \cdot \vec{\theta}_1 \rangle$ and $\langle \hat{\phi}_2 \cdot \vec{\theta}_3 \rangle$ are large by construction. All the others are much smaller. This shows again the generally random nature of the flux. The directions of the vectors in the 1,2 plane demonstrate the simple tendency of flux that enters the cube through one face to leave it through others. In $U(1)\times U(1)\times U(1)$, the flux is conserved while the SU(2) data show large deviations from Abelian conservation.

However, there is a Bianchi identity[1,4,6] for the SU(2) theory that constrains the flux vectors. This identity reduces to simple Abelian conservation as $\beta \to \infty$, but it is complicated at finite β when expressed in terms of $\vec{\theta}$ variables. Thus, while the SU(2) patterns are no less constrained than those of $U(1)\times U(1)\times U(1)$, they are allowed to be more complicated.

The orientations of the flux vectors along the $\hat{\phi}_3$ direction in the pictures have been explained above. They are arranged so as to reduce the flux through compound routes such as the one in Fig. 8.

There is a relationship between the averages presented here and the $\langle \vec{\theta}_1 \cdot \vec{\theta}_j \rangle$ studied in I. A rough guess that neglects certain correlations is

$$\langle \vec{\theta}_1 \cdot \vec{\theta}_j \rangle \cong \langle |\vec{\theta}_1| \rangle \langle \hat{\theta}_1 \cdot \vec{\theta}_j \rangle . \quad (4.5)$$

At weak coupling, both sides behave as β^{-1} and the coefficients differ by 15%. Equation (4.5) is a reasonable guide.

The quantities of central interest in I were

$$D = \left\langle \vec{\theta}_1 \cdot \sum_{j=1}^{6} \vec{\theta}_j \right\rangle \quad (4.6)$$

and

$$R = \langle \vec{\theta}_1 \cdot \vec{\theta}_4 \rangle / \langle \vec{\theta}_1 \cdot \vec{\theta}_3 \rangle . \quad (4.7)$$

D was loosely interpreted as a density of magnetic sources and R as a rough indication of the shape of the flux pattern. The measurements of D indicated the presence of significant non-Abelian effects. Several manifestations of this have already been seen here. Equation (4.5) suggests that

$$\langle \hat{\phi}_1 \cdot \vec{\theta}_1 \rangle \left\langle \hat{\phi}_1 \cdot \sum \vec{\theta}_j \right\rangle \quad (4.8)$$

will be close to D. This is found to be true. More generally, all the $\langle \hat{\phi}_i \cdot \sum \vec{\theta}_j \rangle$ are qualitatively the same as D in measurement and interpretation.

In spite of these non-Abelian effects, R was observed to stay surprisingly close to its weak-coupling value down to the crossover region. As (4.5) would suggest, $\langle \hat{\phi}_1 \cdot \vec{\theta}_4 \rangle / \langle \hat{\phi}_1 \cdot \vec{\theta}_3 \rangle$ has similar behavior. We have no explanation for the especially close correspondence between this ratio and its weak-coupling limit. It seems anomalous amid the other non-Abelian effects.

In the $U(1)\times U(1)\times U(1)$ data, all the $\langle \hat{\phi}_i \cdot \sum \vec{\theta}_j \rangle$ are zero to many places. Only monopoles can contribute here. Thus, the data confirm the expectation that such objects are very sparse at these β values.

V. CONCLUSIONS

Although the flux patterns are too random to view directly, some simple averages reveal the correlations and these can be represented in pictures. The fluctuations in the non-Abelian theory are larger and more disordered than those of the Abelian standards. The SU(2) theory takes advantage of its more complicated configuration space [as compared with that of $U(1)\times U(1)\times U(1)$] to manifest significant non-Abelian effects in the flux pattern even at large β.

ACKNOWLEDGMENTS

This research was supported by the Alfred P. Sloan Foundation and the Department of Energy. Help with the numerical work was generously provided by the Stanford Linear Accelerator Center and the University of California at Davis high-energy experimental group. K.S. thanks W. Iley for a helpful conversation.

[1]J. Kiskis, Phys. Rev. D **28**, 2637 (1983).
[2]For a recent review see M. Creutz, L. Jacobs, and C. Rebbi, Phys. Rep. **95**, 201 (1983).
[3]J. Ambjørn and P. Olesen, Nucl. Phys. **B170** [FS1],60 (1980); H. B. Nielsen and P. Olesen, Report No. NBI-HE-79-45 (unpublished); G. Parisi, in *High Energy Physics—1980,* proceedings of the XXth International Conference, Madison, Wisconsin, edited by L. Durand and L. G. Pondrom (AIP, New York, 1981); P. Olesen, Nucl. Phys. **B200** [FS4], 381 (1982).
[4]J. Kiskis, Phys. Rev. D **26**, 429 (1982).
[5]B. Baaquie, Phys. Rev. D **16**, 2612 (1977).
[6]G. Batrouni, Nucl. Phys. **B208**, 467 (1982).
[7]D. G. Caldi, Nucl. Phys. **B220** [FS8], 48 (1983).